energies

MDPI

Article

Photovoltaic Performance of Dye-Sensitized Solar Cells with a Solid-State Redox Mediator Based on an Ionic Liquid and Hole-Transporting Triphenylamine Compound

Minseon Kong †, Da Hyeon Oh †, Baekseo Choi and Yoon Soo Han *

Department of Advanced Materials and Chemical Engineering, Daegu Catholic University, Gyeongsan-si 38430, Korea; qewr1666@naver.com (M.K.); ws5963@naver.com (D.H.O.); skdiwlsdnr@naver.com (B.C.)

* Correspondence: yshancu@cu.ac.kr

† These authors contributed equally to this work.

Abstract: An ionic liquid, 1-methyl-3-propylimidazolium iodide (MPII), was solidified with an organic hole-transporting material, 4,4′,4″-tris[(3-methylphenyl)phenylamino]triphenylamine (m-MTDATA), and the resulting solid-state redox mediator (RM) (m-MTDATA-solidified MPII) was employed in solar devices to realize solid-state dye-sensitized solar cells (sDSSCs). Solar devices with only MPII or m-MTDATA as an RM showed almost 0 mA/cm^2 of short-circuit current (J_{sc}) and thus 0% power conversion efficiency (PCE). However, an sDSSC with the m-MTDATA-solidified MPII exhibited 4.61 mA/cm^2 of J_{sc} and 1.80% PCE. It was found that the increased J_{sc} and PCE were due to the formation of I_3^-, which resulted from a reaction between the iodie (I^-) of MPII and m-MTDATA cation. Further enhancement in both J_{sc} (9.43 mA/cm^2) and PCE (4.20%) was observed in an sDSSC with 4-tert butylpyridine (TBP) as well as with m-MTDATA-solidified MPII. We attributed the significant increase (about 230%) in PCE to the lowered diffusion resistance of I^-/I_3^- ions in the solid-state RM composed of the m-MTDATA-solidified MPII and TBP, arising from TBP's role as a plasticizer.

Keywords: dye-sensitized solar cell; solid-state redox mediator; ionic liquid; 4-tert butylpyridine; m-MTDATA

Citation: Kong, M.; Oh, D.H.; Choi, B.; Han, Y.S. Photovoltaic Performance of Dye-Sensitized Solar Cells with a Solid-State Redox Mediator Based on an Ionic Liquid and Hole-Transporting Triphenylamine Compound. *Energies* **2022**, *15*, 2765. https://doi.org/10.3390/en15082765

Academic Editors: Alessandro Cannavale and Ubaldo Ayr

Received: 19 February 2022
Accepted: 6 April 2022
Published: 9 April 2022

1. Introduction

A conventional dye-sensitized solar cell (DSSC) typically comprises an organic-solvent-based liquid redox mediator (RM) and two electrodes (i.e., dye-adsorbed TiO_2 photoanode and Pt-coated counter electrode). It has a three-layered structure in which the liquid RM is sandwiched between the two electrodes [1–4]. For the last three decades, numerous studies have been performed, and a power conversion efficiency (PCE) as high as 14.3% has been achieved [5]. However, the potential problems caused by organic-solvent-based liquid RMs, such as their leakage, the volatilization of solvents at high temperatures, and the precipitation of salts at low temperature, are considered critical reasons for limiting the commercialization and practicable use of DSSCs [6]. By replacing the liquid RM with a solid-state (s) RM or hole-transporting material (HTM) in DSSCs, the above problems can be solved, and dye desorption can also be prevented [7]. There are two types of sDSSCs: one is a sandwich-structured cell with a basic configuration of glass/F-doped tin oxide (FTO)/mesoporous TiO_2:dye/sRM/platinized FTO/glass, and the other is a metal-back-contact-structured device with a configuration of glass/FTO/mesoporous TiO_2:dye/sHTM/metal electrodes (Au or Ag). The sandwich-structured sDSSCs include several-micrometer-thick sRM layers. Therefore, they are disadvantageous in improving PCE compared to the metal-back-contact-structured sDSSCs, in which the thickness of sHTM layers is typically under 1 μm.

Recently, photovoltaic properties of sandwich-structured sDSSCs have been reported [8–12]. When inorganic sRMs, such as $CsSnI_{2.95}F_{0.05}$ doped with SnF_2 [8] and Cs_2SnI_6 with additives [9], were applied, sandwich-structured sDSSCs showed PCEs of up to 10.2% and 7.8%, respectively. It has also been reported that PCEs of sandwich-structured sDSSCs ranged from 5.68% to up to 11%, when metal complexes ($Cu^{2+/+}$ or $Co^{3+/2+}$) in combination with lithium bis(trifluoromethanesulfonyl)imide (LiTFSI) and 4-tert-butylpyridine (TBP) [or 4-(trifluoromethyl)pyridine] were employed as sRMs [10–12]. As another approach to creating sRMs for sandwich-structured sDSSCs, the solidification of ionic liquids has been attempted [13–19]. Ionic liquid, a salt in liquid state at room temperature, features high ionic conductivity, negligible vapor pressure, high thermal stability, and a wide electrochemical window [6,15]. Dialkylimidazolium iodides, such as 1-methyl-3-propylimidazolium iodide (MPII), 1-butyl-3-methylimidazolium iodide (BMII), and 1-ethyl-3-methylimidazolium iodide (EMII), have been used for the liquid and/or sRMs of DSSCs as an iodide (I^-) source. These ionic liquids were solidified by mixing them with conductors, semiconductors, or insulators to apply them to sRMs for sDSSCs. A 5.4% PCE was achieved in a sandwich-structured sDSSC when MPII in combination with LiTFSI and TBP was cast on a solid-state polymerized poly(3,4-ethylenedioxythiophene) (P3HT) as a solidifying agent [13]. In addition, several ionic liquid/solidifier systems, such as MPII (without I_2)/polyaniline-loaded carbon black (5.81%) [6], BMII + $BMISO_3CF_3$(with I_2)/SiO_2 (4.83%) [14], BMII(with I_2)/TiC (1.68%) [15], EMITFSI + EMII(with I_2)/SiO_2 (3.7%) [16], $BMIBF_4$(with I_2)/silica (4.98%) [17], EMITFSI + EMII(with I_2)/TiO_2 (5.0%) [18], EMITFSI + EMII(with I_2)/carbon fiber (4.97%) [18], and MPII(with I_2)/silica (7.0%) [19], were also reported. In most of these reports, iodine (I_2) was added to solidified ionic liquid systems to produce triiodide (I_3^-) via a reaction with the iodide (I^-) [14–19]. However, the corrosive nature of iodine can limit the use of metallic-grid electrodes in the manufacturing of multi-cell modules [6,13].

This study aims at providing an iodine-free and volatile-organic-solvent-free sRM, which applies to even several-micrometer-thick hole transporting layers for applications to sandwich-structured sDSSCs. We prepared an iodine-free sRM based on an ionic liquid (MPII) as an iodide source and a hole-transporting triphenylamine compound, 4,4′,4″-tris[phenyl(*m*-tolyl)amino]triphenylamine (m-MTDATA), as a solidifier. m-MTDATA is one of the most well-known arylamine compounds applied in organic light-emitting diodes and perovskite solar cells as a hole injection or transporting material, and devices with m-MTDATA have shown good performance [20–22]. Compared with polymeric solidifiers such as P3HT [13] and polyaniline [6], low-molecular-weight m-MTDATA is highly advantageous in terms of pore-filling property because polymers are poorly penetrated into the TiO_2 mesopores, which arises from mismatches between the polymer and mesopore sizes. Uniform pore-filling property is essential to ensuring higher PCEs of DSSCs. The viscous liquid of MPII was solidified with m-MTDATA by simply mixing them and then applying them to sDSSCs as an sRM. We fabricated sandwich-structured sDSSCs with the solidified MPII, and their photovoltaic performance was investigated. To the best of our knowledge, sandwich-structured sDSSCs with m-MTDATA-solidified MPII as an sRM have never been reported. The reported photovoltaic parameters [i.e., short-circuit current density (J_{sc}), open-circuit voltage (V_{oc}), fill factor (*FF*) and PCE] of sandwich-structured sDSSCs with solidified ionic liquid are summarized in Table 1, including those of our device with the m-MTDATA-solidified MPII.

Table 1. Reported photovoltaic performance of sandwich-structured sDSSCs with an sRM based on ionic liquids and solidifying agents.

Ionic Liquids	Solidifying Agents	J_{sc} (mA/cm^2)	V_{oc} (V)	FF (%)	PCE (%)	Ref.
MPII (without I_2)	P3HT	14.2	0.64	60	5.4	[13]

Table 1. *Cont.*

Ionic Liquids	Solidifying Agents	J_{sc} (mA/cm^2)	V_{oc} (V)	FF (%)	PCE (%)	Ref.
MPII (without I_2)	polyaniline-loaded carbon black	12.20	0.737	65	5.81	[6]
MPII (without I_2)	m-MTDATA	9.43	0.610	73.0	4.20	This study
BMII + $BMISO_3CF_3$ (with I_2)	SiO_2	11.3	-	-	4.83	[14]
BMII (with I_2)	TiC	3.40	0.6686	74	1.68	[15]
EMITFSI + EMII (with I_2)	SiO_2	10.4	0.592	62	3.7	[16]
$BMIBF_4$ (with I_2)	Silica	8.60	0.621	69.9	4.98	[17]
EMITFSI + EMII (with I_2)	TiO_2	11.45	0.675	65	5.00	[18]
EMITFSI + EMII (with I_2)	Carbon fiber	11.11	0.688	65	4.97	[18]
MPII (with I_2)	Silica	13.67	0.700	73.1	7.0	[19]

2. Experimental Details

2.1. Materials

FTO glass with a sheet resistance of ~7 Ω/square (TCO22-7), TiO_2 paste for the mesoporous layer (Ti-nanoxide T/SP), TiO_2 paste for the scattering layer (Ti-nanoxide R/SP), N719 dye (Ruthenizer 535-bisTBA), and hot-melt adhesive (Metlonix 1170-25, DuPont Surlyn) were purchased from Solaronix (Aubonne, Switzerland). Titanium diisopropoxide bis(acetylacetonate) (TPA), $TiCl_4$, MPII, m-MTDATA, TBP, and LiTFSI were procured from Sigma-Aldrich (St. Louis, MO, USA). Platinum paste (PT-1) from Dyesol-Timo JV (Seoul, Korea) was selected as the source for the Pt-coated counter electrode. All of the chemicals for DSSC fabrications were used without further purification.

2.2. Fabrication of Sandwich-Structured sDSSCs

Except for the preparation of the sRM, the same procedures mentioned in our previous reports were employed to fabricate working (glass/FTO/TiO_2:dye) and counter (glass/platinized FTO) electrodes for sandwich-structured sDSSCs [23,24]. A 25-µm-thick hot-melt adhesive was sandwiched between the working and counter electrodes and then annealed for 10 min at 120 °C to seal the two electrodes.

The preparation processes of the sRM are as follows: m-MTDATA (50 mg) as a solidifying agent was dissolved in 1 mL of chloroform. An ionic liquid solution was separately prepared by dissolving MPII (1 M, 252 mg) in 1 mL of chloroform. For comparison, TBP- and TBP/LiTFSI-containing ionic liquid solutions were also prepared by adding TBP (0.2 M, 27 mg) and TBP (0.2 M, 27 mg)/LiTFSI (0.066 M, 19 mg) into the MPII solution, respectively. The m-MTDATA and ionic liquid solutions were mixed with a volume ratio of 3:1 to apply to the sRM. The mixed solutions were then injected into the sealed cells through a pre-drilled hole formed on the counter electrodes, and the cells were dried in a vacuum oven for 60 min at 50 °C. The injection and drying process was repeated four times to fully fill a space between the mesoporous TiO_2 layer and the platinized FTO layer, thereby fabricating sandwich-structured sDSSCs with a 25 mm^2 active area. The detailed fabrication conditions of sandwich-structured sDSSCs are provided in the electronic supplementary information (ESI).

2.3. Fabrication of Hole-Only Devices

Hole-only devices (HODs) with a layer configuration of glass/platinized FTO/TiO_2:N719 dye/sRM with or without additives/platinized FTO/glass were fabricated using the same procedures presented in our earlier work [24]. The detailed fabrication conditions are provided in the ESI.

2.4. Measurements

The cross-sectional morphology of the sandwich-structured sDSSCs was visualized via field-emission scanning electron microscopy (FE–SEM; S-4800, Hitachi High-Technology; Tokyo, Japan) equipped with energy-dispersive X-ray spectroscopy (EDS) (Horiba EX-250, Horiba; Kyoto, Japan). The photocurrent–voltage measurements were performed using a CompactStat potentiostat (Ivium Technologies B.V.; Eindhoven, The Netherlands) and a PEC-L01 solar simulator system equipped with a 150-W xenon arc lamp (Peccell Technologies, Inc.; Yokohama, Japan). The light intensity was adjusted to 1 sun (100 mW/cm^2) using a silicon photodiode (PEC-SI01, Peccell Technologies, Inc.; Yokohama, Japan). The monochromatic incident-photon-to-current conversion efficiencies (IPCEs) were plotted as a function of light wavelength using an IPCE measurement instrument (PEC-S20, Peccell Technologies, Inc.; Yokohama, Japan). The UV–vis absorption spectra were obtained using a SINCO NEOSYS-2000 spectrophotometer (Seoul, Korea). Electrochemical impedance spectroscopic (EIS) analyses were performed using an electrochemical analyzer (CompactStat, Ivium Technologies B.V.; Eindhoven, The Netherlands). The active areas of the dye-adsorbed TiO_2 films were estimated using a digital microscope camera (SZ61, OLYMPUS Corporation; Tokyo, Japan) equipped with image analysis software.

3. Results and Discussion

3.1. Photovoltaic Performance of sDSSCs with m-MTDATA-Solidified MPII

We could prepare the sRM composed of MPII (iodide source) and m-MTDATA (solidifier) by simply mixing and drying the corresponding solutions, i.e., a viscous liquid phase of MPII was solidified with a solid powder of m-MTDATA. As shown in Figure S1 of the ESI, the viscous flow behavior of MPII disappeared by mixing it with m-MTDATA. In addition, a solid-state was maintained when additives (TBP and LiTFSI) were added to the m-MTDATA-solidified MPII. We first investigated the pore-filling property of the solidifier (m-MTDATA) into TiO_2 layers in DSSCs. As shown in Figure 1, carbon atoms from the low-molecular-weight m-MTDATA are uniformly distributed throughout the TiO_2 layer. This is beneficial to obtain higher PCE in DSSCs due to effective hole collection at the counter electrode and dye regeneration near the TiO_2:dye layer. In our previous report, the pore-filling into the TiO_2 layers was not completed when polymeric hole-transporting materials were used [24].

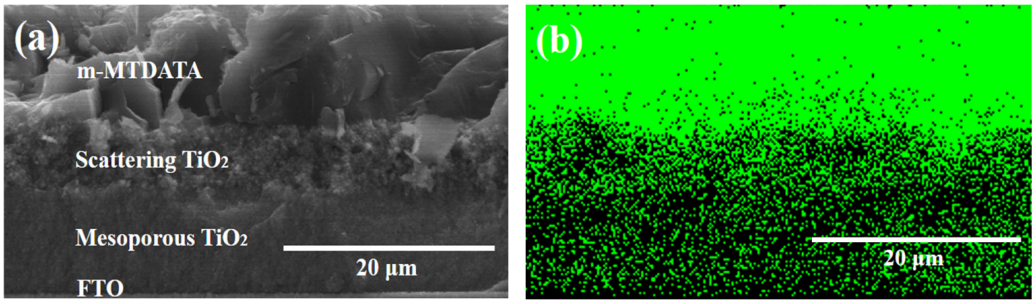

Figure 1. Cross-sectional SEM (**a**) and EDS mapping images showing the distribution of carbon (**b**) in a decapped sDSSC with m-MTDATA. N719 dyes containing carbon atoms were not adsorbed on TiO_2 surface.

Using the MPII, m-MTDATA, or m-MTDATA-solidified MPII, sandwich-structured DSSCs with or without additives were fabricated, as shown in Table 2, and their photo-

voltaic properties were investigated. The average photovoltaic properties measured using four cells are compared in Figure 2 and Table 3, and their raw data are presented in Table S1 of the ESI. Solar devices with only MPII (DSSC-a) or m-MTDATA (sDSSC-b) showed 0.22 ± 0.05 and 0% PCE, respectively; on the other hand, a significant increase in average PCE (1.42 ± 0.42%) was observed in the sDSSC-c with m-MTDATA-solidified MPII. When TBP was added to m-MTDATA-solidified MPII, the average PCE value (3.75 ± 0.43%) of the sDSSC-d was further increased compared to that of the sDSSC-c without TBP. Unexpectedly, by additional incorporation of LiTFSI as well as TBP into the m-MTDATA-solidified MPII, the photovoltaic performance (1.50 ± 0.12%) of the sDSSC-e was again decreased from that of the sDSSC-d.

Table 2. Fabricated DSSCs with five different types of RM for comparison.

Solar Cells	Components of RM	Phase of RM
DSSC-a	MPII	Viscous liquid
sDSSC-b	m-MTDATA	Solid powder
sDSSC-c	MPII, m-MTDATA	Solid-state (nonfluidic composite)
sDSSC-d	MPII, m-MTDATA, TBP	Solid-state (nonfluidic composite)
sDSSC-e	MPII, m-MTDATA, TBP, LiTFSI	Solid-state (nonfluidic composite)

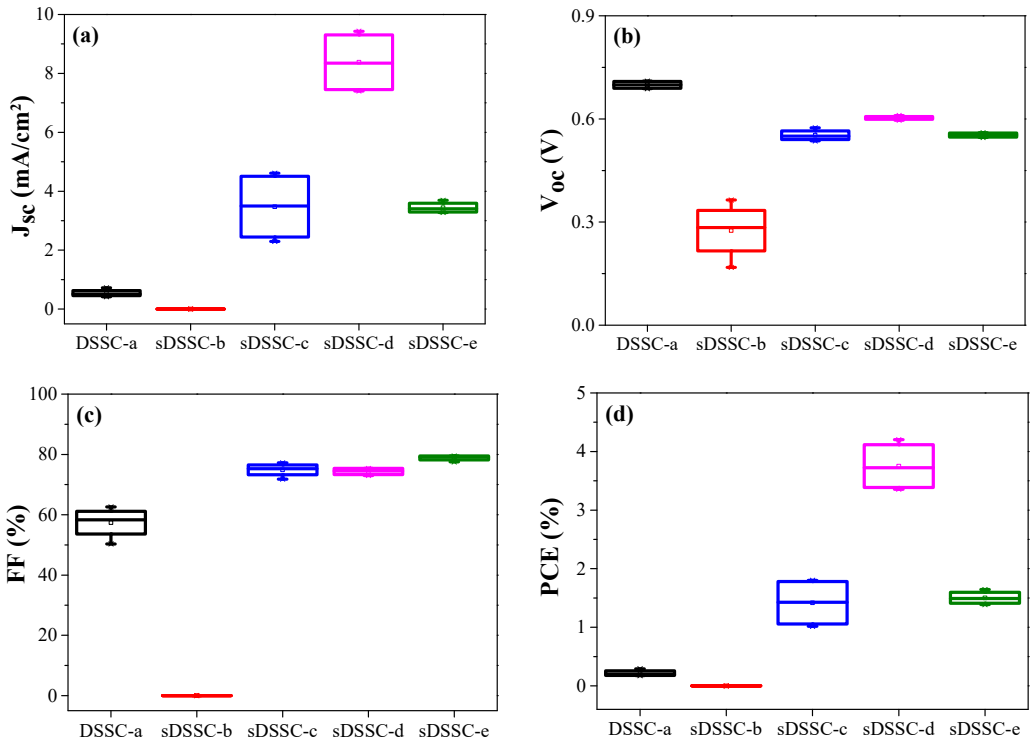

Figure 2. Box plots for photovoltaic performance of the DSSCs with five different types of RM; (**a**) J_{sc}, (**b**) V_{oc}, (**c**) *FF*, and (**d**) PCE measured under the AM 1.5 condition.

Among the four cells prepared in each condition, we selected the champion cells to compare their photovoltaic properties. Here, we denote the champion cell with the m-MTDATA-solidified MPII by sDSSC-c'. The same denotation is applied for the champion sDSSC-d and e. Figure 3a,b shows the current density (*J*)-voltage (*V*) and dark-current curves of the champion devices, respectively, and their photovoltaic parameters are listed in Table 4. Photovoltaic performance largely varied with the types of RM, i.e., PCEs ranged from 0% to 4.20%. We investigated the origins of the performance variations, and the examination results are described in detail in the following sections.

Table 3. Averages and standard deviations of cell performance measured using four cells with five different types of RM.

Solar Cells	J_{sc} (mA/cm^2)	V_{oc} (V)	*FF* (%)	PCE (%)
DSSC-a	0.54 ± 0.13	0.722 ± 0.052	57.38 ± 5.25	0.22 ± 0.05
sDSSC-b	0.001 ± 0.002	0.275 ± 0.082	0	0
sDSSC-c	3.48 ± 1.20	0.553 ± 0.017	74.90 ± 2.30	1.42 ± 0.42
sDSSC-d	8.38 ± 1.08	0.603 ± 0.006	74.34 ± 1.19	3.75 ± 0.43
sDSSC-e	3.45 ± 0.19	0.553 ± 0.007	78.82 ± 0.91	1.50 ± 0.12

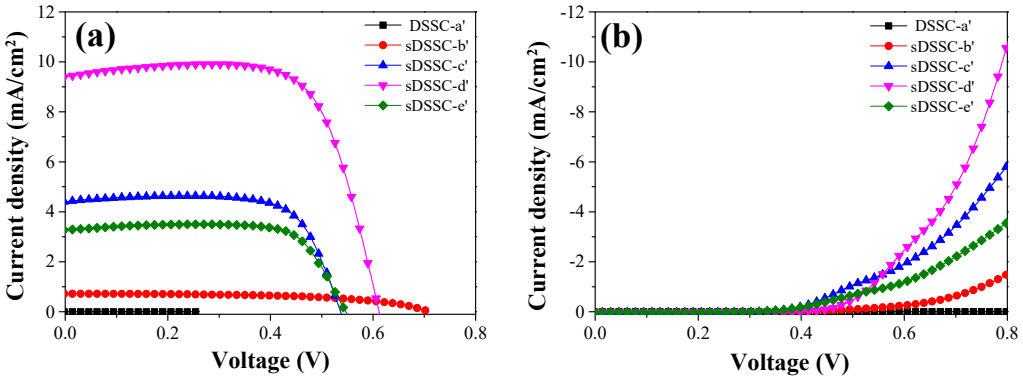

Figure 3. *J–V* characteristics (**a**) and dark-current (**b**) curves for the champion devices with MPII, m-MTDATA, or solidified MPII layer with or without additives.

Table 4. Photovoltaic performance of champion cells with MPII, m-MTDATA, or solidified MPII layer with or without additives.

Champion Cells	J_{sc} (mA/cm^2)	V_{oc} (V)	FF (%)	PCE (%)
DSSC-a′	0.72	0.708	56.86	0.29
sDSSC-b′	0.004	0.304	0	0
sDSSC-c′	4.61	0.544	71.81	1.80
sDSSC-d′	9.43	0.610	73.03	4.20
sDSSC-e′	3.28	0.546	77.53	1.39

3.2. Hole Conduction Mechanism in sDSSCs with m-MTDATA-Solidified MPII

As mentioned earlier, DSSCs with only MPII or m-MTDATA showed almost 0 mA/cm^2 of J_{sc} and thus 0% PCE. In the DSSC-a′ with MPII, triiodide (I_3^-) was barely present in the RM because iodine (I_2) was not added [25]. This fact indicates that hole transportation from the oxidized dye to the platinized counter electrode cannot be completed, leading to very low J_{sc} and PCE. In the case of the sDSSC-b′ with m-MTDATA, hole conduction cannot occur because the carrier diffusion length in a solid organic semiconductor is very short, typically around 100 nm [24,26,27]. When considering that the layer thickness of m-MTDATA in the sDSSC-b′ is about 10.6 µm (Figure S2 of the ESI), effective hole transportation is impossible, inducing approximately 0 mA/cm^2 of J_{sc}. However, the sDSSC-c′ with the m-MTDATA-solidified MPII as an RM exhibited 4.61 mA/cm^2 of J_{sc} and 1.80% PCE (Table 4). By adopting the m-MTDATA-solidified MPII, the PCE of the sDSSC-c′ was significantly enhanced compared to that of the DSSC-a′ (only MPII) or the sDSSC-b′ (only m-MTDATA). This tendency for variations in the J_{sc} value is quite consistent with that in the dark currents, as shown in Figure 3b.

It is important to elucidate the origins of the considerable improvement in the photovoltaic performance of the sDSSC-c′. Figure 4 depicts the UV-visible absorption spectra of

MPII and m-MTDATA solutions in chloroform. The MPII solution exhibited an absorption peak at 245 nm, attributable to iodide (I^-) [28,29], and two absorption peaks at 316 nm and 345 nm were observed from the m-MTDATA solution [20,30]. Surprisingly, the absorbance of the two peaks derived from m-MTDATA was increased by adding pure MPII to the m-MTDATA solution, even though the concentration of m-MTDATA was maintained. It has been reported that the absorption peaks of triiodide (I_3^-) are around 290 nm and 360 nm [28,29]. The triiodide's absorption regions are substantially overlapped with the two absorptions peaks of m-MTDATA. We thus noticed that the increased absorbance at both 316 nm and 345 nm was due to the generation of triiodide by any reaction between MPII and m-MTDATA. Meanwhile, although the concentration of MPII in the MPII/m-MTDATA mixture was increased, the absorbance at 316 nm and 345 nm was not further increased. In contrast, the absorbance of iodide (MPII) at 245 nm was increased, as shown in Figure S3 of the ESI. This fact also indicates that the increase in absorbance (at 316 nm and 345 nm) for the MPII/m-MTDATA mixture, compared to that of the pristine m-MTDATA, is not attributable to MPII but instead to the triiodide produced by a chemical reaction between MPII and m-MTDATA. To obtain other evidence of the triiodide formation, IPCEs of the sDSSC-c' were measured as a function of wavelength. Relatively low IPCE at around 360 nm is generally observed in I^-/I_3^--based DSSCs, because triiodides (I_3^-) absorb the 360 nm light, and therefore N719 dye cannot effectively absorb the light [28]. As displayed in Figure S4 of the ESI, a valley ranging from 350 to 400 nm was observed in the IPCE spectrum of the sDSSC-c', indicating the presence of triiodides in the sRM (i.e., m-MTDATA-solidified MPII) layer.

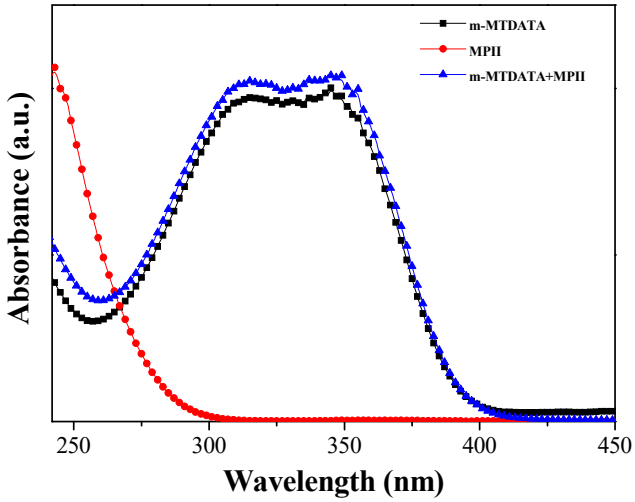

Figure 4. UV–visible absorption spectra of MPII, m-MTDATA, and their mixture in chloroform.

A possible mechanism for triiodide formation can be explained by chemical reactions (1)–(4): m-MTDATA can absorb near UV and blue regions of visible light and can then be excited, as expressed in reaction (1). The excited m-MTDATA reacts with the oxygen molecules infiltrated during the fabrication of cells, and therefore m-MTDATA cations and oxygen anions are formed. It is known that the reduction potential of oxygen molecules is −0.35 V versus a normal hydrogen electrode (NHE) [31], and the lowest-unoccupied-molecular-orbital (LUMO) energy level of m-MTDATA is −2.0 eV of the absolute vacuum scale (AVS) [32], corresponding to −2.5 V versus NHE ($E_{AVS} = -E_{NHE} - 4.50$ eV) [33]. Thus, reaction (2) can occur spontaneously because of the low-lying energy level of oxygen molecules compared to the LUMO level of m-MTDATA. Similar results, i.e., reactions between excited semiconductors and oxygen gases, have been reported [34–36]. Finally, triiodides can be formed via reaction (3) between m-MTDATA cations and some parts of iodides (MPII), and thereby they exist throughout the RM (m-MTDATA-solidified MPII) layer. This occurs because the highest-occupied-molecular-orbital energy level of m-MTDATA

(0.60 V versus NHE or 5.1 eV versus AVS) is approximately 0.25 V higher than the reduction potential of the I^-/I_3^- redox couple (0.35 V versus NHE). Reaction (4) means that the generated oxygen anions can be stabilized with the imidazolium cations (MPI^+) to a certain degree. Overall, by mixing MPII and m-MTDATA, triiodides were formed in the m-MTDATA-solidified MPII. The residual (unreacted) I^- and the produced I_3^- led to the completion of the hole conduction, i.e., the dye regeneration ($3I^- + 2D^+ \rightarrow I_3^- + 2D$, where D indicates N719 dye), near the TiO_2:dye layer and the hole collection ($I_3^- + 2e^- \rightarrow 3I^-$) at the platinized counter electrode. As another contribution to hole conduction, m-MTDATA can transport holes from oxidized dyes to platinized counter electrodes. As presented in Equation (2), oxidized species (m-$MTDATA^+$) was formed by a reaction between m-MTDATA and oxygen molecule, resulting in p-doping of m-MTDATA. This indicated that holes were presented throughout the sRM layer under illumination, enhancing conductivity and faster hole mobility [34].

$$2\text{m-MTDATA} + h\nu \rightarrow 2\text{m-MTDATA}^* \quad (1)$$

$$2\text{m-MTDATA}^* + 2O_2 \rightarrow 2\text{m-MTDATA}^+ + 2O_2^- \quad (2)$$

$$2\text{m-MTDATA}^+ + 3I^- \rightarrow 2\text{m-MTDATA} + I_3^- \quad (3)$$

$$2MPI^+ + 2O_2^- \rightarrow 2MPI^+ \cdots O_2^- \quad (4)$$

Meanwhile, oxygen molecules permeated into cells during their fabrication can cause the degradation of organic semiconductors [37,38]. It has been reported that the quantum yield for degradation of N719 dye bound on TiO_2 surfaces increases with increasing amounts of oxygen molecules, probably due to the generation of active oxygen species. Thus, oxygen gases in the cells can function as beneficial p-dopant and a harmful medium for dye degradation.

3.3. Effects of Additives on Performance of sDSSCs with m-MTDATA-Solidified MPII

In both metal-back-contact-structured and sandwich-structured sDSSCs, additives such as TBP and LiTFSI were widely utilized for improving photovoltaic performance [7,9–13]. To examine the effects of TBP and LiTFSI incorporated into the m-MTDATA-solidified MPII, we fabricated the sDSSC-d and the sDSSC-e (Table 2), and photovoltaic performance was compared, as shown in Figure 3 and Table 4. By incorporating TBP into the m-MTDATA-solidified MPII, a PCE of 4.20% (J_{sc} = 9.43 mA/cm^2, V_{oc} = 0.610 V, and FF = 73.03%) was achieved in the sDSSC-d', which corresponded to a 230% enhancement in efficiency compared to that (1.80%) of the sDSSC-c' without TBP. It has been reported that TBP can be adsorbed onto the free area of the TiO_2 surface, resulting in the shifting of the TiO_2's conduction band edge (CBE) to a negative direction [39]. This negative shift of the CBE can lead to an increase in V_{oc} due to a broadened potential gap between the CBE (TiO_2) and the redox potential (electrolyte) and a decrease in J_{sc} due to a reduced electron injection efficiency [23,39]. However, in this study, by the addition of TBP, the J_{sc} value was dramatically increased, from 4.61 mA/cm^2 for the sDSSC-c to 9.43 mA/cm^2 for the sDSSC-d. As a reference, weight ratios of TBP, m-MTDATA, and MPII in the sDSSC-d' were calculated to be 6.0, 37.9, and 56.1 wt%, respectively. We attributed the large increase (around 205%) in J_{sc} in the sDSSC-d' to the plasticizer effect of TBP. In other words, it was considered that the liquid phase of TBP (T_m = −41.0 °C) at room temperature played the role of a plasticizer in the m-MTDATA-solidified MPII. When a small amount of bulky TBP (6.0 wt% or 8.7 vol%) was added to the m-MTDATA-solidified MPII, it could be inserted between the m-MTDATA molecules, thereby broadening the distance between the solidifying agents. This could induce the faster diffusion of both I^- and I_3^- through the m-MTDATA-modified MPII layer.

To confirm this, we conducted EIS analysis for the sDSSC-c', the sDSSC-d', and the sDSSC-e'. The Nyquist plots of the EIS spectra for the sDSSCs measured under AM 1.5 one-sun illumination are shown in Figure 5, providing the sheet resistance (R_s) and interface

resistances [40]. Three distinct semicircles were observed. The first and second semicircles corresponded to the carrier transport resistances at the Pt/RM (R_1) and TiO_2/N719/RM (R_2) interfaces, respectively. The last semicircle was ascribed to the Warburg diffusion resistance (w_1) for the ionic transport within the RM. The fitted resistances using Z-view software are compared in Table 5. The w_1 value of the sDSSC-d′ with TBP was lowered to 22.02 Ω from 46.98 Ω of the sDSSC-c′ without TBP. By adding TBP, the ionic diffusion resistance was largely decreased, indicating that more efficient ion (I^- and I_3^-) diffusions between the Pt counter electrode and the dye-adsorbed TiO_2 layer were accomplished in the sDSSC-d′. This fact suggests that TBP acts as a plasticizer in the m-MTDATA-solidified MPII. As a result, redox reactions, such as the dye regeneration ($3I^- + 2D^+ \rightarrow I_3^- + 2D$) near the TiO_2:dye layer and the hole collection [$I_3^- + 2e^-$ (Pt) $\rightarrow 3I^-$] at the platinized counter electrode, can occur more effectively. This can lower both R_1 and R_2 values in the sDSSC-d, as shown in Table 5. Eventually, the sharp reduction in the ionic diffusion resistance in the DSSC-d′, compared to that in the sDSSC-c′, induced about a 205% increase in J_{sc} (Table 4). As a reference, when the EIS measurement is conducted under illumination (open-circuit condition), the R_2 value is affected by the entire resistances, i.e., the electron injection from excited dyes to the conduction band of TiO_2 (R_{inj}), transportation through TiO_2 layer (R_{tra}), recombination between injected electron and electrolyte (R_{rec}), and dye regeneration (R_{reg}). The R_{inj}, R_{rec}, and R_{reg} values are relatively low because electrons move to lower energy levels. However, in the case of R_{tra}, electrons move through the same energy level of TiO_2. Thus, when the EIS measurement is conducted at open-circuit voltage (under illumination), the R_2 value almost depends on the electron transfer resistance [41–43]. As tabulated in Table 5, a lower R_2 value (15 Ω) in the sDSSC-d′ indicates a more efficient charge transfer through the TiO_2 layer, and, thereby, a lower recombination rate between photoinjected electrons and sRM, compared to those of sDSSC-c′ and e′.

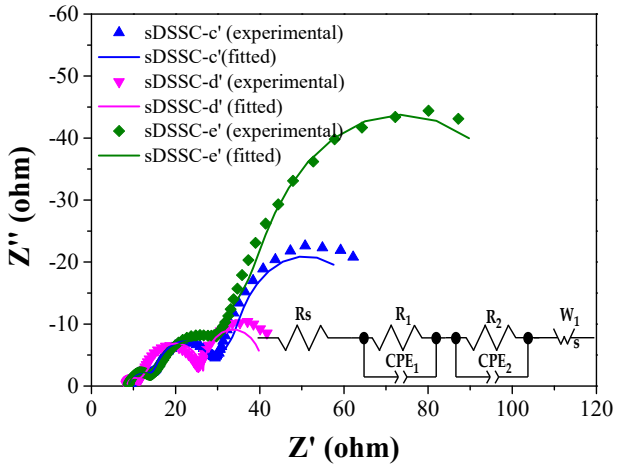

Figure 5. Nyquist plots of EIS spectra for the sDSSC-c′, sDSSC-d′, and sDSSC-e′, measured in an open-circuit condition under the illumination of simulated AM 1.5 solar light. Inset shows the equivalent circuit for sDSSCs; where CPE indicates constant phase element.

Table 5. Fitted resistances for the sDSSC-c′, sDSSC-d′, and sDSSC-e′ based on the m-MTDATA-solidified MPII with or without additives.

Champion Cells	Additive	R_s (Ω)	R_1 (Ω)	R_2 (Ω)	w_1 (Ω)
sDSSC-c′	None	8.36	7.43	19.78	46.98
sDSSC-d′	TBP	8.39	4.41	15.00	22.02
sDSSC-e′	TBP and LiTFSI	8.89	6.53	29.39	103.81

Meanwhile, it has been reported that LiTFSI as a p-dopant can increase conductivity and hole mobility when it is doped in various organic small-molecular and polymeric

HTMs [34,35,44]. We thus fabricated the sDSSC-e with an sRM composed of m-MTDATA-solidified MPII, TBP, and LiTFSI, and compared its photovoltaic performance to that of the sDSSC-d without LiTFSI. The PCE of the sDSSC-e' was decreased from that of the sDSSC-d', mainly due to a decrement in J_{sc} (Table 4). In addition, the ion diffusion resistance surged with the addition of LiTFSI (Table 5). We first considered that the LiTFSI addition would lead to an improvement in cell performance by its doping effect, but a decrement in PCE was observed in the sDSSC-e' with LiTFSI. Xiong and Meng et al. reported that a wax-like complex was formed by mixing TBP with LiTFSI via an interaction between Li^+ (LiTFSI) and a nonbonding electron pair of nitrogen (TBP). The TBP-LiTFSI complex could alleviate the hygroscopicity of LiTFSI and the corrosive effect of TBP, achieving enhanced device efficiency and stability [44]. From this point of view, it is believed that TBP and LiTFSI form a wax-like complex in the sDSSC-e', and thus TBP can no longer act as a plasticizer. As a result, we can attribute the decreased PCE and increased diffusion resistance to the formation of a wax-like TBP-LiTFSI complex in the sDSSC-e'.

To further confirm the influence of additives (TBP and LiTFSI), we fabricated HOD-c (with m-MTDATA-solidified MPII), HOD-d (with m-MTDATA-solidified MPII and TBP), and HOD-e (with m-MTDATA-solidified MPII, TBP, and LiTFSI), and their *J-V* characteristics were measured. *J-V* curves of HODs fabricated using three different sRMs are shown in Figure S5 of the ESI. We selected the best-performing HODs among 3 devices in each condition to compare their *J-V* properties. As compared in Figure 6, by incorporating TBP into m-MTDATA-solidified MPII, dark currents of the HOD-d' were sharply increased from those of the HOD-c' without TBP, indicating that TBP acted as a plasticizer in m-MTDATA-solidified MPII. Furthermore, dark currents of the HOD-e' were again decreased by adding LiTFSI, probably due to the formation of wax-like TBP-LiTFSI complexes, causing a loss of TBP's function as a plasticizer. These tendencies in the dark currents of the HODs were quite consistent with the J_{sc} values of their counterparts, i.e., sDSSC-c', sDSSC-d', and sDSSC-e'.

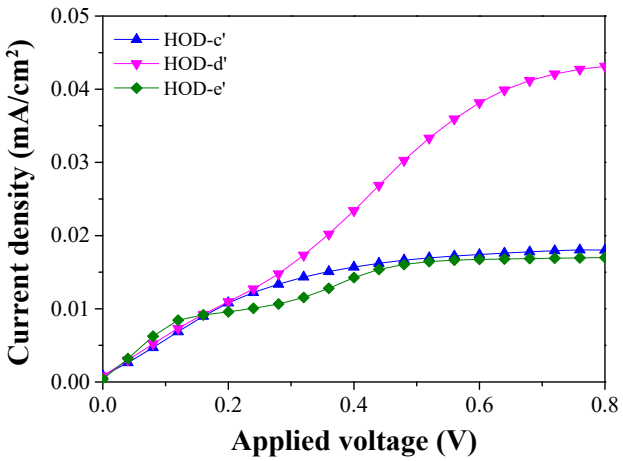

Figure 6. *J-V* characteristics of the HOD-c', HOD-d', and HOD-e'.

Figure 7 compares IPCE spectra for the champion cells such as sDSSC-c', d', and e'. As can be expected, higher IPCEs were recorded in the sDSSC-d' by incorporation of TBP into the sDSSC-c' with m-MTDATA-solidified MPII. IPCE values of the sDSSC-e' were again reduced by adding LiTFSI. The tendencies of IPCE variations with additives were well consistent with the measurement results of the J_{sc} values (Figure 3a), dark currents (Figure 3b), interface resistances (Figure 5), and HOD's dark currents (Figure 6).

As a result, the highest PCE of 4.20% in an sDSSC was achieved by adopting an sRM composed of m-MTDATA-solidified MPII and TBP. Although this efficiency was lower than those of iodine-free P3HT/MPII (5.40%) [13] and polyaniline-loaded carbon black/MPII (5.81%) [6], this study's result has great importance. It is because the efficiency was accomplished in sandwich-structured sDSSCs, in which the thickness of the hole-

transporting layer was approximately 10 μm as shown in Figure S2. In P3HT/MPII-based sDSSC, adhesives for sealing working and counter electrodes were not used, and thus TiO_2 photoanode was directly contacted with a counter electrode, allowing very short ion diffusion length [13]. In sDSSC with polyaniline-loaded carbon black/MPII, carbon blacks coated on counter electrode functioned electrical conductive pathway from counter electrode to TiO_2 photoanode, and therefore ion diffusion length could be minimized [6]. Overall, it is believed that the PCE of 4.20% is an impressive achievement because it is extracted from the sDSSC with a 10 μm-thick hole transporting layer.

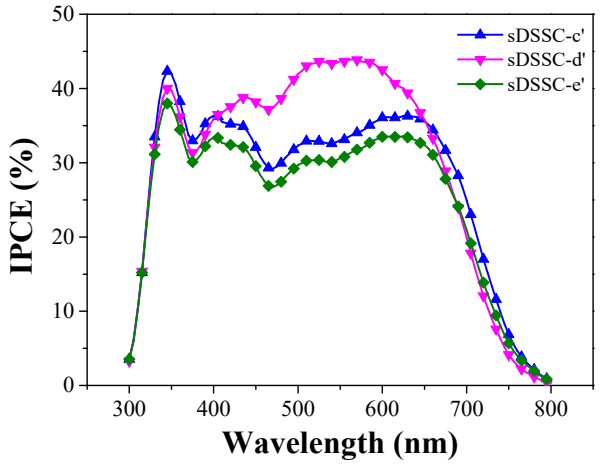

Figure 7. IPCE spectra for sDSSC-c′, d′ and e′ as a function of wavelength.

4. Conclusions

An sRM based on an ionic liquid (MPII) and a hole-transporting triphenylamine compound (m-MTDATA) was successfully prepared and applied for applications to sDSSCs. The sDSSC-c′ with the m-MTDATA-solidified MPII showed a PCE of 1.80% with 4.61 mA/cm^2 of J_{sc}, 0.544 V of V_{oc}, and 71.81% of *FF*. The UV-visible absorption and IPCE studies disclosed that a chemical reaction between MPII and m-MTDATA cation resulted in the formation of triiodides (I_3^-), allowing hole conduction from the oxidized dye to the counter electrode. In addition, by incorporating TBP as an additive into the m-MTDATA-solidified MPII, the PCE of the sDSSC-d′ was sharply increased by 4.20% (J_{sc} = 9.43 mA/cm^2, V_{oc} = 0.610 V, and *FF* = 73.03%), due to improvements in all photovoltaic parameters, and the ion diffusion resistance was considerably decreased. These results were ascribed to the plasticizer effect of the bulky-structured TBP. As a result, the sRM composed of m-MTDATA-solidified MPII and TBP appears to be a promising material for replacing conventional organic-solvent-based liquid RMs, and thereby for realizing the sDSSCs.

Supplementary Materials: The following supporting information can be downloaded at https://www.mdpi.com/article/10.3390/en15082765/s1. Figure S1: Photographs of redox mediators; (a) MPII, (b) m-MTDATA-solidified MPII (MPII + m-MTDATA), (c) m-MTDATA-solidified MPII + TBP, and (d) m-MTDATA-solidified MPII + TBP + LiTFSI. Table S1: Photovoltaic parameters of DSSCs with five different types of redox mediator. Figure S2: Cross-sectional SEM image of the sDSSC-b′ with only m-MTDATA. Figure S3: Absorbance variations of the m-MTDATA/MPII mixtures with increasing concentrations of MPII; the concentration of m-MTDATA in the mixture was constant. For comparison, the absorption spectra of m-MTDATA and MPII were included. Figure S4: IPCE spectrum of the sDSSC-c′ with m-MTDATA-solidified MPII. The arrow-marked valley ranging from 350 to 400 nm was attributed to absorption by I_3^- ions in sRM (i.e., m-MTDATA-solidified MPII) layer. Figure S5: Dark current density-voltage characteristics of HODs with three different types of RM; (a) HOD-c with m-MTDATA-solidified MPII, (b) HOD-d with m-MTDATA-solidified MPII/TBP, and (c) HOD-e with m-MTDATA-solidified MPII/TBP/LiTFSI.

Author Contributions: Conceptualization, Y.S.H.; methodology, M.K. and D.H.O.; formal analysis, M.K., D.H.O. and B.C.; writing—original draft preparation, Y.S.H.; writing—review and editing, Y.S.H.; funding acquisition, Y.S.H. All authors have read and agreed to the published version of the manuscript.

Funding: This work was supported by research grants from Deagu Catholic University in 2021 (20211058).

Data Availability Statement: Data are contained within the article or the Supplementary Material.

Conflicts of Interest: The authors declare no conflict of interest. The funders had no role in the design of the study; in the collection, analyses, or interpretation of data; in the writing of the manuscript; or in the decision to publish the results.

References

1. O'Regan, B.; Grätzel, M. A low-cost, high-efficiency solar cell based on dye-sensitized colloidal TiO_2 films. *Nature* **1991**, *353*, 737–740. [CrossRef]
2. Gong, J.; Sumathy, K.; Qiao, Q.; Zhou, Z. Review on dye-sensitized solar cells (DSSCs): Advanced techniques and research trends. *Renew. Sustain. Energ. Rev.* **2017**, *68*, 234–246. [CrossRef]
3. Sharma, K.; Sharma, V.; Sharma, S.S. Dye-sensitized solar cells: Fundamentals and current status. *Nanoscale Res. Lett.* **2018**, *13*, 381. [CrossRef] [PubMed]
4. Devadiga, D.; Selvakumar, M.; Shetty, P.; Santosh, M.S. Recent progress in dye sensitized solar cell materials and photo-supercapacitors: A review. *J. Power Sources* **2021**, *493*, 229698. [CrossRef]
5. Kakiage, K.; Aoyama, Y.; Yano, T.; Oya, K.; Fujisawa, J.I.; Hanaya, M. Highly-efficient dye-sensitized solar cells with collaborative sensitization by silyl-anchor and carboxy-anchor dyes. *Chem. Commun.* **2015**, *51*, 15894–15897. [CrossRef]
6. Lee, C.P.; Chen, P.Y.; Vittal, R.; Ho, K.C. Iodine-free high efficient quasi solid-state dye-sensitized solar cell containing ionic liquid and polyaniline-loaded carbon black. *J. Mater. Chem.* **2010**, *20*, 2356–2361. [CrossRef]
7. Benesperi, I.; Michaels, H.; Freitag, M. The researcher's guide to solid-state dye-sensitized solar cells. *J. Mater. Chem.* **2018**, *6*, 11903–11942. [CrossRef]
8. Chung, I.; Lee, B.; He, J.; Chang, R.P.H.; Kanatzidis, M.G. All-solid-state dye-sensitized solar cells with high efficiency. *Nature* **2012**, *485*, 486–489. [CrossRef]
9. Lee, B.; Stoumpos, C.C.; Zhou, N.; Hao, F.; Malliakas, C.; Yeh, C.Y.; Marks, T.J.; Kanatzidis, M.G.; Chang, R.P.H. Air-stable molecular semiconducting iodosalts for solar cell applications: Cs_2SnI_6 as a hole conductor. *J. Am. Chem. Soc.* **2014**, *136*, 15379–15385. [CrossRef]
10. Cao, Y.; Saygili, Y.; Ummadisingu, A.; Teuscher, J.; Luo, J.; Pellet, N.; Giordano, F.; Zakeeruddin, S.M.; Moser, J.E.; Freitag, M.; et al. 11% efficiency solid-state dye-sensitized solar cells with copper(II/I) hole transport materials. *Nat. Commun.* **2016**, *8*, 15390. [CrossRef]
11. Freitag, M.; Daniel, Q.; Pazoki, M.; Sveinbjornsson, K.; Zhang, J.; Sun, L.; Hagfeldt, A.; Boschloo, G. High-efficiency dye-sensitized solar cells with molecular copper phenanthroline as solid hole conductor. *Energy Environ. Sci.* **2015**, *8*, 2634–2637. [CrossRef]
12. Kashif, M.K.; Milhuisen, R.A.; Nippe, M.; Hellerstedt, J.; Zee, D.Z.; Duffy, N.W.; Halstead, B.; Angelis, F.D.; Fantacci, S.; Fuhrer, M.S.; et al. Cobalt polypyridyl complexes as transparent solution-processable solid-state charge transport materials. *Adv. Energy Mater.* **2016**, *6*, 1600874. [CrossRef]
13. Koh, J.K.; Kim, J.; Kim, B.; Kim, J.H.; Kim, E. Highly efficient, iodine-free dye-sensitized solar cells with solid-state synthesis of conducting polymers. *Adv. Mater.* **2011**, *23*, 1641–1646. [CrossRef] [PubMed]
14. Lee, K.M.; Chen, P.Y.; Lee, C.P.; Ho, K.C. Binary room-temperature ionic liquids based electrolytes solidified with SiO_2 nanoparticles for dye-sensitized solar cells. *J. Power Sources* **2009**, *190*, 573–577. [CrossRef]
15. Lee, C.P.; Lee, K.M.; Chen, P.Y.; Ho, K.C. On the addition of conducting ceramic nanoparticles in solvent-free ionic liquid electrolyte for dye-sensitized solar cells. *Sol. Energy Mater. Sol. Cells* **2009**, *93*, 1411–1416. [CrossRef]
16. Katakabe, T.; Kawano, R.; Watanabe, M. Acceleration of redox diffusion and charge-transfer rates in an ionic liquid with nanoparticle addition. *Electrochem. Solid-State Lett.* **2007**, *10*, F23–F25. [CrossRef]
17. Chen, Z.; Yang, H.; Li, X.; Li, F.; Yi, T.; Huang, C. Thermostable succinonitrile-based gel electrolyte for efficient, long-life dye-sensitized solar cells. *J. Mater. Chem.* **2007**, *17*, 1602–1607. [CrossRef]
18. Usui, H.; Matsui, H.; Tanabe, N.; Yanagida, S. Improved dye-sensitized solar cells using ionic nanocomposite gel electrolytes. *J. Photochem. Photobiol. A Chem.* **2004**, *164*, 97–101. [CrossRef]
19. Wang, P.; Zakeeruddin, S.M.; Comte, P.; Exnar, I.; Grätzel, M. Gelation of ionic liquid-based electrolytes with silica nanoparticles for quasi-solid-state dye-sensitized solar cells. *J. Am. Chem. Soc.* **2003**, *125*, 1166–1167. [CrossRef]
20. Shan, M.; Jiang, H.; Guan, Y.; Sun, D.; Wang, Y.; Hua, J.; Wang, J. Enhanced hole injection in organic light-emitting diodes utilizing a copper iodide-doped hole injection layer. *RSC Adv.* **2017**, *7*, 13584–13589. [CrossRef]
21. Kim, J.Y.; Kwak, G.; Choi, Y.C.; Kim, D.H.; Han, Y.S. Enhanced performance of perovskite solar cells by incorporation of a triphenylamine derivative into hole-transporting poly(3-hexylthiophene) layers. *J. Ind. Eng. Chem.* **2019**, *73*, 175–181. [CrossRef]

22. Liu, C.; Zhang, D.; Li, Z.; Zhang, X.; Shen, L.; Guo, W. Efficient 4,4′,4″-tris(3-methylphenylphenylamino)triphenylamine (m-MTDATA) hole transport layer in perovskite solar cells enabled by using the nonstoichiometric precursors. *Adv. Funct. Mater.* **2018**, *28*, 1803126. [CrossRef]
23. Baek, G.W.; Kim, Y.J.; Jung, K.H.; Han, Y.S. Enhancement of solar cell performance through the formation of a surface dipole on polyacrylonitrile-treated TiO_2 photoelectrodes. *J. Ind. Eng. Chem.* **2019**, *73*, 260–267. [CrossRef]
24. Kong, M.; Kim, K.S.; Nga, N.V.; Lee, Y.; Jeon, Y.S.; Cho, Y.; Kwon, Y.; Han, Y.S. Molecular weight effects of biscarbazole-based hole transport polymers on the performance of solid-state dye-sensitized solar cells. *Nanomaterials* **2020**, *10*, 2516. [CrossRef]
25. Boschloo, G.; Hagfeldt, A. Characteristics of the iodide/triiodide redox mediator in dye-sensitized solar cells. *Acc. Chem. Res.* **2009**, *42*, 1819–1826. [CrossRef] [PubMed]
26. Longeaud, C.; Allah, A.F.; Schmidt, J.; Yaakoubi, M.E.; Berson, S.; Lemaitre, N. Determination of diffusion lengths in organic semiconductors: Correlation with solar cell performances. *Org. Electron.* **2016**, *31*, 253–257. [CrossRef]
27. Mikhnenko, O.V.; Blom, P.W.M.; Nguyen, T.Q. Exciton diffusion in organic semiconductors. *Energy Environ. Sci.* **2015**, *8*, 1867–1888. [CrossRef]
28. Kim, M.J.; Lee, C.R.; Jeong, W.S.; Im, J.H.; Ryu, T.I.; Park, N.G. Unusual enhancement of photocurrent by incorporation of bronsted base thiourea into electrolyte of dye-sensitized solar cell. *J. Phys. Chem.* **2010**, *114*, 19849–19852. [CrossRef]
29. Bonomo, M.; Carlo, A.D.; Dini, D. Study of the influence of the I-based electrolyte composition on the photoconversion properties of p-type dye-sensitized solar cell. *J. Electrochem. Soc.* **2018**, *165*, H889–H896. [CrossRef]
30. Sakurai, M.; Kabe, R.; Fuki, M.; Lin, Z.; Jinnal, K.; Kobori, Y.; Adachi, C.; Tachikawa, T. Organic photostimulated luminescence associated with persistent spin-correlated radical pairs. *Commun. Mater.* **2021**, *2*, 74. [CrossRef]
31. Koppenol, W.H.; Stanbury, D.M.; Bounds, P.L. Electrode potentials partially reduced oxygen species, from dioxygen to water. *Free Radic. Biol. Med.* **2010**, *49*, 317–322. [CrossRef] [PubMed]
32. Chulkin, P.; Lapkowski, M.; Bryce, M.R.; Santos, J.; Data, P. Determination of standard redox rate constants of OLED active compounds by electrochemical impedance spectroscopy. *Electrochim. Acta* **2017**, *258*, 1160–1172. [CrossRef]
33. Sung, H.K.; Lee, Y.; Kim, W.H.; Lee, S.J.; Sung, S.J.; Kim, D.H.; Han, Y.S. Enhanced power conversion efficiency dye-sensitized solar cells by band edge shift of TiO_2 photoanode. *Molecules* **2020**, *25*, 1502. [CrossRef] [PubMed]
34. Abate, A.; Leijtens, T.; Pathak, S.; Teusher, J.; Avolio, R.; Errico, M.E.; Kirkpatrik, J.; Ball, J.M.; Docampo, P.; McPherson, I.; et al. Lithium salts as "redox active" p-type dopants for organic semiconductors and their impact in solid-state dye-sensitized solar cells. *Phys. Chem. Chem. Phys.* **2013**, *15*, 2575–2579. [CrossRef]
35. Cappel, U.B.; Daeneke, T.; Bach, U. Oxygen-induced doping of spiro-MeOTAD in solid-state dye-sensitized solar cells and its impact on device performance. *Nano Lett.* **2012**, *12*, 4925–4931. [CrossRef]
36. Xu, B.; Gabrielsson, E.; Safdari, M.; Cheng, M.; Hua, Y.; Tian, H.; Gardner, J.M.; Kloo, L.; Sun, L. 1,1,2,2-Tetrachloroethane (TeCA) as a solvent additive for organic hole transport materials and its application in highly efficient solid-state dye-sensitized solar cells. *Adv. Energy Mater.* **2015**, *5*, 1402340. [CrossRef]
37. Quan, V.A. Degradation of the Solar Cell Dye Sensitizer N719 Preliminary Building of Dye-Sensitized Solar Cell. Master's Thesis, Roskide University, Roskide, Denmark, June 2006.
38. Schafferhans, J.; Baumann, A.; Wagernpfahl, A.; Deibel, C.; Dyakonov, V. Oxygen doping of P3HT:PCBM blends: Influence on trap states, charge carrier mobility and solar cell performance. *Org. Electron.* **2010**, *11*, 1693–1700. [CrossRef]
39. Kusama, H.; Arakawa, H. Influence of aminotriazole additives in electrolytic solution on dye-sensitized solar cell performance. *J. Photochem. Photobio. A Chem.* **2004**, *164*, 103–110. [CrossRef]
40. Shaikh, S.F.; Mane, R.S.; Min, B.K.; Hwang, Y.J.; Joo, O.S. D-sorbitol-induced phase control of TiO_2 nanoparticles and its application for dye-sensitized solar cells. *Sci. Rep.* **2016**, *6*, 20103. [CrossRef]
41. Xu, J.; Fan, K.; Shi, W.; Li, K.; Peng, T. Application of ZnO micro-flowers as scattering layer for ZnO-based dye-sensitized solar cells with enhanced conversion efficiency. *Sol. Energy* **2014**, *101*, 150–159. [CrossRef]
42. Park, J.H.; Kim, J.Y.; Kim, J.H.; Choi, C.J.; Kim, H.; Sung, Y.E.; Ahn, K.S. Enhanced efficiency of dye-sensitized solar cells through $TiCl_4$-treated, nanoporous-layer-covered TiO_2 nanotube arrays. *J. Power Sources* **2011**, *196*, 8904–8908. [CrossRef]
43. Ambade, S.B.; Ambade, R.B.; Mane, R.S.; Lee, G.W.; Shaikh, S.F.; Patil, S.A.; Joo, O.S.; Han, S.H.; Lee, S.H. Low temperature chemically synthesized rutile TiO_2 photoanodes with high electron lifetime for organic dye-sensitized solar cells. *Chem. Commun.* **2013**, *49*, 2921–2923. [CrossRef] [PubMed]
44. Wang, S.; Huang, Z.; Wang, X.; Li, Y.; Gunther, M.; Valenzuela, S.; Parikh, P.; Cabreros, A.; Xiong, W.; Meng, Y.S. Unveiling the role of tBP−LiTFSI complexes in perovskite solar cells. *J. Am. Chem. Soc.* **2018**, *140*, 16720–16730. [CrossRef] [PubMed]